Cell. Mol. Life Sci. (2011) 68:1065–1077
DOI 10.1007/s00018-010-0508-2

Cellular and Molecular Life Sciences

RESEARCH ARTICLE

Kinetic and structural evidence of the alkenal/one reductase specificity of human ζ-crystallin

Sergio Porté · Agrin Moeini · Irene Reche · Naeem Shafqat · Udo Oppermann · Jaume Farrés · Xavier Parés

Received: 17 June 2010 / Revised: 4 August 2010 / Accepted: 10 August 2010 / Published online: 11 September 2010

Abstract Human ζ-crystallin is a Zn^{2+}-lacking medium-chain dehydrogenase/reductase (MDR) included in the quinone oxidoreductase (QOR) family because of its activity with quinones. In the present work a novel enzymatic activity was characterized: the double bond α,β-hydrogenation of medium-chain 2-alkenals and 3-alkenones. The enzyme is especially active with lipid peroxidation products such as 4-hydroxyhexenal, and a role in their detoxification is discussed. This specificity is novel in the QOR family, and it is similar to that described in the distantly related alkenal/one reductase family. Moreover, we report the X-ray structure of ζ-crystallin, which represents the first structure solved for a tetrameric Zn^{2+}-lacking MDR, and which allowed the identification of the active-site lining residues. Docking simulations suggest a role for Tyr53 and Tyr59 in catalysis. The kinetics of Tyr53Phe and Tyr59Phe mutants support the implication of Tyr53 in binding/catalysis of alkenal/one substrates, while Tyr59 is involved in the recognition of 4-OH-alkenals.

Keywords Alkenal/one reductase · Quinone oxidoreductase · Lipid peroxidation products · Double-bond α,β-hydrogenation · Medium-chain dehydrogenases/reductases

S. Porté · A. Moeini · I. Reche · J. Farrés · X. Parés (✉)
Department of Biochemistry and Molecular Biology,
Faculty of Biosciences, Universitat Autònoma de Barcelona,
08193 Bellaterra, Barcelona, Spain
e-mail: xavier.pares@uab.es

N. Shafqat · U. Oppermann
Structural Genomics Consortium, University of Oxford,
Old Road Research Campus,
Oxford OX3 7DQ, UK

U. Oppermann
Botnar Research Center,
NIHR Oxford Biomedical Research Unit, Oxford OX3 7DQ, UK

Introduction

ζ-Crystallin is a member of the medium-chain dehydrogenase/reductase (MDR) superfamily [1] and was described initially as a protein found in high amount in guinea pig and camel lenses [2]. A mutation in guinea pig ζ-crystallin gene is associated with congenital development of cataracts [3]. It has been proposed that guinea pig ζ-crystallin could be implicated in the regulation of NADPH homeostasis or it could have a role related to its quinone oxidoreductase activity [4].

Quinone oxidoreductase activity serves to name a group of proteins [5, 6] constituting a complex protein family (QOR) that comprises, along with other families, the Zn^{2+}-lacking MDRs. These proteins are much less studied than the Zn^{2+}-containing MDRs, and they are classified into three major protein families: QOR, enoyl thioester reductase (ETR), and alkenal/one reductase (AOR). Each family includes different subfamilies sharing low sequence identity [7]. The physiological role of ETRs and AORs seems to be related to double-bond hydrogenation, their enzymatic activity being *trans*-2-enoyl reductase and α-β unsaturated aldehyde/ketone reductase, respectively. Structural data and mutagenesis studies of ETRs and AORs suggest the participation of a tyrosine residue in their enzymatic activity. In contrast, the physiological role of QOR remains unclear and no catalytic mechanism has been proposed for any member of this enzyme family. Its so far uniquely described enzymatic activity is the reduction of quinones using exclusively NADPH as a cofactor. These quinones are mainly in the *ortho* configuration, and activity

has been demonstrated only for a few members: mammalian ζ-crystallin [8], QORs from bacteria [9, 10], archea [11] and yeast [8], and p53-inducible gene 3 protein (PIG3) [12]. This enzymatic activity suggests that QORs may act as detoxification enzymes, although this has not been demonstrated in vivo, and it has even been proposed that PIG3 may act as a prooxidant enzyme implicated in the induction of apoptosis [12]. However, some QORs are induced by oxidative stress [8, 10], reinforcing their potential role in detoxification pathways.

In addition to its enzymatic role, ζ-crystallin can act as a nucleic acid-binding protein. Bovine and *Pichia pastoris* ζ-crystallins are able to bind to single-stranded DNA, and this binding is disrupted by NADPH competition [13, 14]. Moreover, ζ-crystallin from rat, human and yeast seem to be involved in posttranscriptional regulation through their ability to bind adenine-uracil-rich elements, which are implicated in mRNA stabilization [8]. Thus, it has been proposed that ζ-crystallin from rat may mediate the regulation of glutaminase and glutamate dehydrogenase mRNA [15, 16]. Recently, it has been reported that ζ-crystallin overexpression and its RNA silencing have an important impact on B-cell lymphoma 2 protein (bcl-2) and bumetanide-sensitive cotransporter type 1 (BSC-1) mRNA stability [17, 18].

In the present work, we identified and characterized a novel enzymatic activity for human ζ-crystallin, the double-bond α,β-hydrogenation of 2-alkenals and 3-alkenones. Such specificity has never been reported for any QOR member, which suggests a new physiological role as a detoxification enzyme of lipid peroxidation products. In addition, we describe the crystallographic structure of human ζ-crystallin, which is the first tetrameric structure ever reported for Zn^{2+}-lacking MDRs. Structural analysis of the active site and site-directed mutagenesis identified amino acids that are important for the specificity towards alkenals/ones.

Materials and methods

Cloning of human ζ-crystallin

Two different constructs were used for heterologous expression. For kinetic characterization and mutagenesis, pET-30 Xa/LIC with ζ-crystallin cDNA, previously obtained by Fernández et al. [8], was used. For protein crystallization, ζ-crystallin cDNA was amplified using primers with ligation-independent cloning sites and cloned into pLIC-SGC1 (GenBank accession no. EF456737), which is a pET-derived vector for IPTG-induced expression. The resulting recombinant protein contained an N-terminal $(His)_6$ tag and a TEV protease cleavage site.

Site-directed mutagenesis

The ζ-crystallin Tyr59Phe mutant was previously prepared by Porté et al. [12] and it was characterized regarding quinone reducing activity. In the present study this mutant was used to investigate the role of Tyr59 in alkenal/one reduction. The ζ-crystallin Tyr53Phe mutant was obtained using ζ-crystallin cDNA cloned into pET30-Xa/LIC as a template [8]. Based on the Quickchange site-directed mutagenesis kit method (Stratagene), we designed two primers (mutated nucleotides are underlined): 5′-CGCT CTGGTACTTTTAGTAGAAAACCACTC-3′ (amino acid positions 55–65) and 5′-GTTTTCTACTAAAAGTACCA GAGCGAATGTATG-3′ (amino acid positions 52–61). All reactions were performed in a DNA thermal cycler (MJ Research) with *Pfu Turbo* DNA polymerase (Stratagene). PCR products were incubated with *Dpn*I at 37°C for 60 min to select against the *dam*-methylated parental strand. The resulting nicked-circular mutagenic strands were transformed into *E. coli* BL21. Prior to expression, DNA was completely sequenced to ensure that unwanted mutations were absent.

Protein expression and purification

Human ζ-crystallin was expressed and purified from the pET-30 Xa/LIC construct as described previously [8]. Human ζ-crystallin from pLIC-SGC1 was expressed in *E. coli* (BL21 Rosetta) in 50 ml Terrific Broth (TB at 5% glucose) in the presence of 100 μg/ml ampicillin and 34 μg/ml chloramphenicol at 37°C overnight. Cells were collected by centrifugation and resuspended into 10 ml prewarmed TB medium (containing 0.05% glucose, 0.2% lactose, 0.06% glycerol, and antibiotics). One aliquot (2.5 ml) of this solution was used to inoculate 2 × 500 ml of the same medium, which was then incubated at 37°C until an OD_{600} of 2 had been reached. Then 1 mM IPTG was added, cells were shifted to room temperature and grown for an additional 20 h. Cells were collected by centrifugation and stored frozen (−20°C) until use. Pellets were resuspended in 20 ml lysis buffer (10 mM imidazole, 300 mM NaCl, 50 mM NaH_2PO_4, pH 8) including Complete, EDTA-free, protease inhibitor cocktail (Roche), lysed by a French pressure cell press, and centrifuged to obtain a clear supernatant (15 min, 20,000×*g*). Supernatants were processed by a two-step chromatographic procedure using an Akta Xpress (GE Healthcare) purification system. In the first step, sample was loaded in a Ni^{2+}-nitrilotriacetic acid His-binding resin (Novagen), washed with buffer (20 mM imidazole, 300 mM NaCl, 50 mM NaH_2PO_4, pH 8) and eluted in elution buffer (250 mM imidazole, 300 mM NaCl, 50 mM NaH_2PO_4, pH 8). The collected peak was injected into a gel-filtration

chromatography system (Superdex S200), and the protein eluting in the main peak was concentrated using an Amicon Ultra device.

Molecular weight determination

The apparent molecular weight of the native enzyme was determined by gel-filtration chromatography on a Shodex KW-803 column (8 × 300 mm) connected to an HPLC system (Waters), and equilibrated with two volumes of 50 mM sodium phosphate, pH 7.0, 0.3 M NaCl. The column was run at a flow rate of 1 ml/min. Calibration was performed with molecular weight markers (Sigma). The subunit structure of the enzyme was determined under denaturing conditions by SDS-polyacrylamide gel electrophoresis and Coomassie-Blue staining.

Kinetic characterization

Activities were determined in 100 mM sodium phosphate, pH 7.5, in the presence of 0.15 mM NADPH, with freshly prepared substrate solutions. Stock quinone, 2-alkenal and 3-alken-2-one solutions were prepared in ethanol, resulting in a final concentration lower than 4% (v/v) ethanol in the assay mixture. All aliphatic unsaturated compounds used as substrates exhibited the *trans* configuration. NADPH kinetic constants were determined in the presence of 0.1 mM 9,10-phenanthrenequinone. The enzymatic activity was measured in a Cary 400 Bio (Varian) spectrophotometer by following the consumption of NADPH at 340 nm ($\varepsilon_{NADPH} = 6{,}200\ M^{-1}\ cm^{-1}$), except for cinnamaldehyde where the activity was monitored at 365 nm ($\varepsilon_{NADPH} = 3{,}510\ M^{-1}\ cm^{-1}$). Controls lacking either substrate or enzyme were run routinely. The reactions started with the addition of the substrate. The initial velocities were measured in duplicate with five different substrate concentrations, and the kinetic constants were calculated using the nonlinear regression program Grafit 5.0 (Eritacus Software). All reported values are expressed as the means ± SE of at least three independent experiments.

GC/MS analysis of reaction products

Reaction mixture (4 ml) contained 4 mM substrate (2-pentenal or 3-penten-2-one), 50 μg purified human ζ-crystallin, 1 mM NADPH, 50 mM glucose-6-phosphate and 10 U glucose-6-phosphate dehydrogenase in 33 mM sodium phosphate, pH 7.0. Glucose-6-phosphate and glucose-6-phosphate dehydrogenase were added to regenerate NADPH. Controls lacking enzyme and potential products (3-penten-2-ol and 2-pentanone for reduction of 3-penten-2-one, 2-pentenol and pentanal for reduction of 2-pentenal) were also analysed. After 16-h incubation at room temperature, the reaction mixture was extracted with 1 ml ethyl acetate. GC/MS analysis was performed using a 6890 Series II GC system (Hewlett-Packard) equipped with a HP5 MS column (30 m × 0.25 mm × 0.25 μm; Agilent Technologies) and a 5973 mass selective detector (Hewlett-Packard). The carrier gas was He at a flow rate of 1 ml/min. The samples were measured in the electron impact mode at 70 eV, using the split injection mode with an injector volume of 0.9 μl and an injector temperature of 250°C. The temperature gradient was 40°C for 8 min, 40–280°C at 40°C min^{-1}, and 280°C for 15 min. The MS was scanned from *m/z* 35–350 and compared with the Wiley Mass Spectral Library database (7th edition).

Crystallization, structure determination and analysis

The structure of human ζ-crystallin was determined by X-ray crystallography (Table 1). Crystals were grown at 20°C in 150-nl sitting drops by mixing 100 nl of protein solution (5 mg/ml) including 5 mM NADPH and 50 nl crystallization solution consisting of 14.4% PEG 10 K, 0.16 M calcium acetate, 20% glycerol, 0.08 M sodium cacodylate, pH 6.5. Data were collected using a rotating anode (Rigaku FR-E SuperBright), and integrated and scaled using DENZO and SCALEPACK. The molecular replacement provided a model which was refined using REFMAC, and finally it was deposited in the PDB with code 1YB5. Structure analysis was done using COOT [19], the PISA server (http://www.ebi.ac.uk/msd-srv/prot_int/pistart.html) [20] and the CASTp [21] server, while figures were prepared with PYMOL (http://www.pymol.org).

Docking simulations

Docking of ζ-crystallin substrates, 2-hexenal, 2-nonenal, 3-nonen-2-one, 4-hydroxy-2-nonenal (HNE) and 4-hydroxy-2-hexenal (HHE), was performed with the program AutoDock 4.0 [22]. Prior to starting simulation, crystallographic ligands and water molecules were removed from the ζ-crystallin structure. The protein molecule was kept rigid, while all the torsional bonds in substrates, except for all the conjugated double bonds, were set free to perform flexible docking. Polar hydrogen atoms were added by using the Hydrogen module in AutoDock Tools, then Gasteiger partial atomic charges were assigned. Each ligand docking was accomplished using 150 Lamarckian genetic algorithm runs starting from a random initial position of the ligand. Following docking all structures generated for the same compound were subjected to cluster analysis with a tolerance of 2.0 Å for an all-atom root mean square deviation (rmsd) from a lower energy structure. A second round of docking was then performed using the global minimum

Table 1 ζ-Crystallin data collection and refinement statistics

	Parameter	Value
Data collection	Space group	$P2_12_12$
	Cell parameters	
	a, b, c (Å)	99.5, 110.2, 77.5
	α, β, γ (°)	90, 90, 90
	Subunits per asymmetric unit	2
	Number of observed reflections	73,050
	Completeness (%)	99.8 (99.5)
	Average $1/\sigma$ (I)	8.4 (57.8)
	R_{sym} (%)	11.5 (2)
Crystallographic refinement	Resolution range (Å)	77.15–1.85 (1.85–1.89)
	R_{work} (%)[a]	17 (30.4)
	R_{free} (%)[b]	20.7 (36)
	Number of observed reflections	71,063 (5,164)
	Ramachandran plot statistics	
	Residues in favoured regions (%)	98.8
	Residues in allowed regions (%)	1.1
	Residues in outlier regions (%)	0.2
	Final model parameters	
	Number of monomers	2
	Residues (each monomer)	324
	Hetero groups (each monomer)	1 $NADP^+$
	Number of water molecules	739
	Average B-factors protein ($Å^2$)	27.9
	Covalent bond lengths (Å)	0.017
	Bond angles (°)	1.57

Values in parenthesis, the last resolution shell

[a] $R_{work} = \sum_{hkl} ||F_{obs}|-|F_{calc}|| / \sum_{hkl} |F_{obs}|$, where F_{obs} and F_{calc} are the observed and calculated structure factors, respectively.

[b] R_{free}: same definition as R_{work} for a cross-validation set of about 5% of the reflections.

structure obtained with a distance of 4 Å or less between the C_β atom of the ligand and the C_4 atom of the nicotinamide ring. We have used multiple docking runs to increase the performance of the docking program [23].

Results

Expression, purification and molecular weight determination of human ζ-crystallin

The protein was expressed in *E. coli* and purified to homogeneity. As has been reported by Fernández et al. [8], human ζ-crystallin is a homotetramer, like camel lens ζ-crystallin [24]. However, this quaternary structure changed with the ionic strength of the chromatography buffer. At 0.3 M NaCl, ζ-crystallin showed a homotetrameric structure, while at 3 M NaCl, it behaved as a dimer in size-exclusion chromatography. This suggests that the interactions between subunits in the tetramer are likely based on electrostatic interactions between charged residues.

Enzymatic characterization of human ζ-crystallin

The quinone-reducing activity of human ζ-crystallin has been characterized previously [8, 12]. In the present study, activity was assayed with 2-alkenals, 3-alken-2-ones, *n*-alkanals and *n*-alkenes in the presence of NADPH as a coenzyme (Table 2) to identify novel substrates. The enzyme showed significant enzymatic activity towards several 2-alkenals and 3-alken-2-ones, although no activity was detected with nonanal and 2-nonene (Table 2), suggesting a specificity towards structures with an α,β-unsaturated bond relative to a carbonyl group. In contrast, the enzyme showed a low level of activity with cinnamaldehyde and no activity with 2-cyclohexen-1-one and 15-ketoprostaglandin E_2. The K_m values for 2-alkenals were in the 0.48–8.6 mM range, while the k_{cat} values were close to 10 min^{-1} (Table 2), except for 4-hydroxy-2-alkenals and propenal (acrolein) which are lipid peroxidation-derived reactive compounds. For this kind of substrate, ζ-crystallin displayed higher k_{cat} values, close to those towards quinones, and lower K_m values, HHE being the best 2-alkenal substrate. The kinetic parameters for

Table 2 Kinetic analysis of human ζ-crystallin

	K_m (μM)	k_{cat} (min^{-1})	k_{cat}/K_m (min^{-1} mM^{-1})
Quinones			
1,2-Naphthoquinone	29 ± 1[a]	170 ± 3[a]	5,900 ± 320[a]
9,10-Phenanthrenequinone	1.5 ± 0.2[a]	130 ± 4[a]	87,000 ± 12,000[a]
2-Alkenals			
Propenal	1,450 ± 200	100 ± 4	70 ± 10
2-Pentenal	8,600 ± 1,100	12 ± 0.6	1.4 ± 0.2
2-Hexenal	5,455 ± 620	17 ± 0.5	3.1 ± 0.4
4-Hydroxy-2-hexenal	130 ± 26	80 ± 5	613 ± 130
2-Nonenal	482 ± 60	6.8 ± 0.2	14 ± 1.8
4-Hydroxy-2-nonenal	550 ± 136	69 ± 7.4	126 ± 34
Cinnamaldehyde	LA	LA	LA
3-Alken-2-ones			
3-Buten-2-one	35 ± 3.5	10 ± 0.2	290 ± 30
3-Penten-2-one	535 ± 34	12 ± 0.2	22 ± 1.5
3-Nonen-2-one	940 ± 260	13 ± 1	14 ± 4
2-Cyclohexen-1-one	NA	NA	NA
Prostaglandins			
15-Ketoprostaglandin E_2	NA	NA	NA.
n-Alkanals			
Nonanal	NA	NA	NA
n-Alkenes			
2-Nonene	NA	NA	NA

NA not active, *LA* low activity (3 nmols/min·mg at 2 m*M* substrate).

Activities were determined in 0.1 M sodium phosphate, pH 7.0, with 0.15 mM NADPH, at 25°C. For k_{cat} calculation, the subunit molecular mass (36 kDa) was used.

All aliphatic unsaturated compounds used as substrates exhibit the *trans* configuration

[a] Fernández et al. [8].

3-alken-2-ones were very similar to those for 2-alkenals, with 3-buten-2-one exhibiting the lowest K_m value (0.035 mM).

Identification of the products from the 2-alkenal and 3-alken-2-one reduction by ζ-crystallin

The reduction reaction of 2-alkenals and 3-alken-2-ones by human ζ-crystallin could generate two potential products: the corresponding alcohol if the carbonyl group was reduced, or the corresponding alkanal/one if the α,β-double bond was reduced (Scheme 1). In order to identify the product and demonstrate the reaction type, GC/MS assays were performed. For the analysis of the 3-alken-2-one reduction, 3-penten-2-one was used as a model substrate, while 2-pentenal was used for the reduction reaction of 2-alkenals. A control reaction lacking enzyme and a mixture of the potential products were also analysed. 3-Penten-2-one was reduced to 2-pentanone (Fig. 1), as shown by coelution with the original compound, as well as by its characteristic MS fragmentation pattern, whereas 2-pentenal was reduced to pentanal (Fig. 2). Thus, the GC/MS results demonstrate that human ζ-crystallin specifically catalyses the reduction of the α,β-unsaturated bond and not the reduction of the carbonyl group.

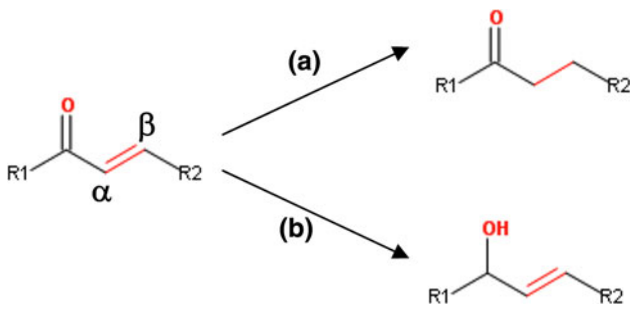

Scheme 1 Potential reduction reactions of alkenal and 3-alken-2-one by ζ-crystallin. Two reaction types could be catalyzed: *a* double-bond α,β-hydrogenation, *b* carbonyl group reduction. *R1* H (alkenal) or C_n (alkenone), *R2* H or C_n

Structure analysis of human ζ-crystallin

With the aim of studying its quaternary structure and the molecular basis for its enzymatic activity, the human ζ-crystallin structure was solved. The overall structure displays the typical MDR fold with two domains: the catalytic domain (residues 1–128 and 271–329) and the coenzyme-binding domain (residues 129–270), which are separated by a deep cleft that binds the cofactor $NADP^+$ and the substrate (Fig. 3a). Although human ζ-crystallin has a low sequence identity with other MDRs of known structure, the main structural features among all MDR proteins are well conserved. The human ζ-crystallin monomer can be superimposed with the *E. coli* QOR

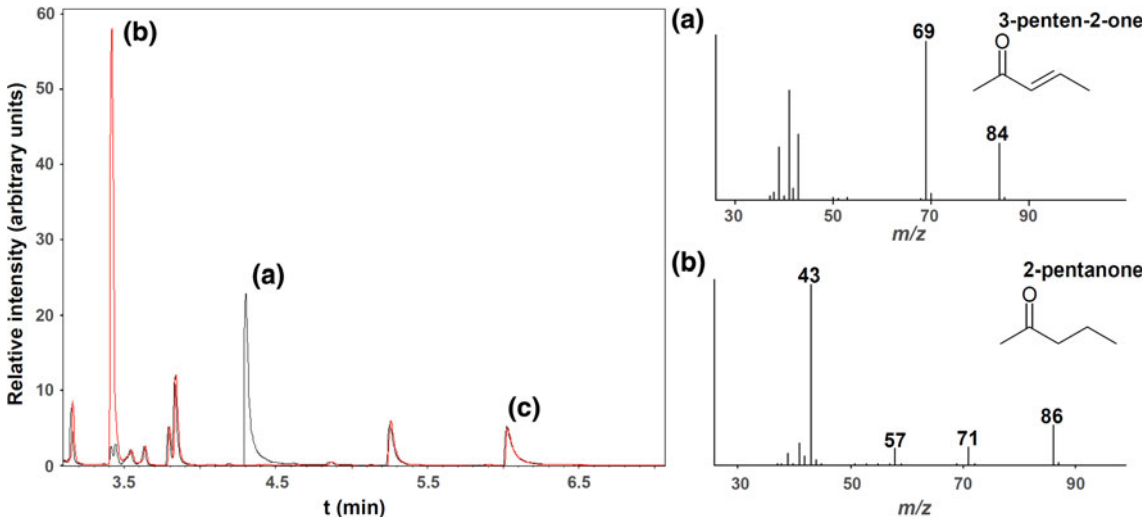

Fig. 1 GC/MS evidence for the selective reduction of the α,β-unsaturated bond of 3-penten-2-one by ζ-crystallin. *Left panel*: superimposition of the chromatograms of the reaction products (in *red*) in the presence of enzyme and control reaction without enzyme (in *black*). *Right panels*: Mass spectra with molecular fragments from peak *a* and peak *b*, which were identified as 3-penten-2-one and 2-pentanone, respectively. Peak *c* was identified as mesytil oxide

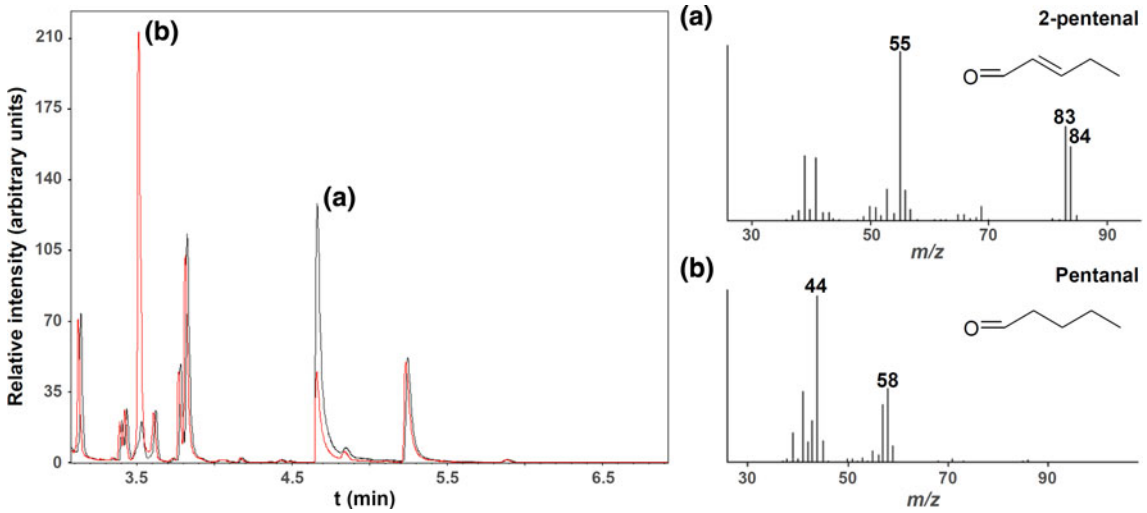

Fig. 2 GC/MS evidence for the selective reduction of the α,β-unsaturated bond of 2-pentenal by ζ-crystallin**.** *Left panel*: superimposition of the chromatograms of the reaction products (in *red*) in the presence of enzyme and control reaction without enzyme (in *black*). *Right panels*: Mass spectra with molecular fragments from peak *a* and peak *b*, which were identified as 2-pentenal and pentanal, respectively

monomer (PDB code 1QOR), which shares 30% sequence identity, with a rmsd of 1.53 Å.

Human ζ-crystallin behaves as a homotetramer. The 1YB5 asymmetric unit contains a dimer designated AB and the biologically active tetramer is generated by crystallographic twofold symmetry. The tetramer can be represented as a dimer of two identical dimers: AB and CD (Fig. 3b), each dimer being similar to the classical horse liver alcohol dehydrogenase dimer. The centre of the tetramer forms a large cavity (20,000 $Å^3$) with an approximate accessible surface area of 7,000 $Å^2$. In each dimer, the monomer–monomer contact occurs along the antiparallel β-strands (β* residues 252–254 and βVI residues 265–268 of each monomer; Fig. 3d). These β-strands are bonded through antiparallel hydrogen bonds with the corresponding sheets of the neighbouring monomer and the subunits associate into a 12-stranded β-sheet (six β-strands of the Rossmann fold motifs in each monomer βI–βVI). The buried accessible surface area per monomer is 1,200 $Å^2$. The interface between dimers is less extensive (buried surface area per monomer is only 600 $Å^2$) and it involves residues of helix αC from the catalytic domain and of helix αa from the coenzyme binding domain. The analysis of interactions between dimers by the PISA server indicates that the only

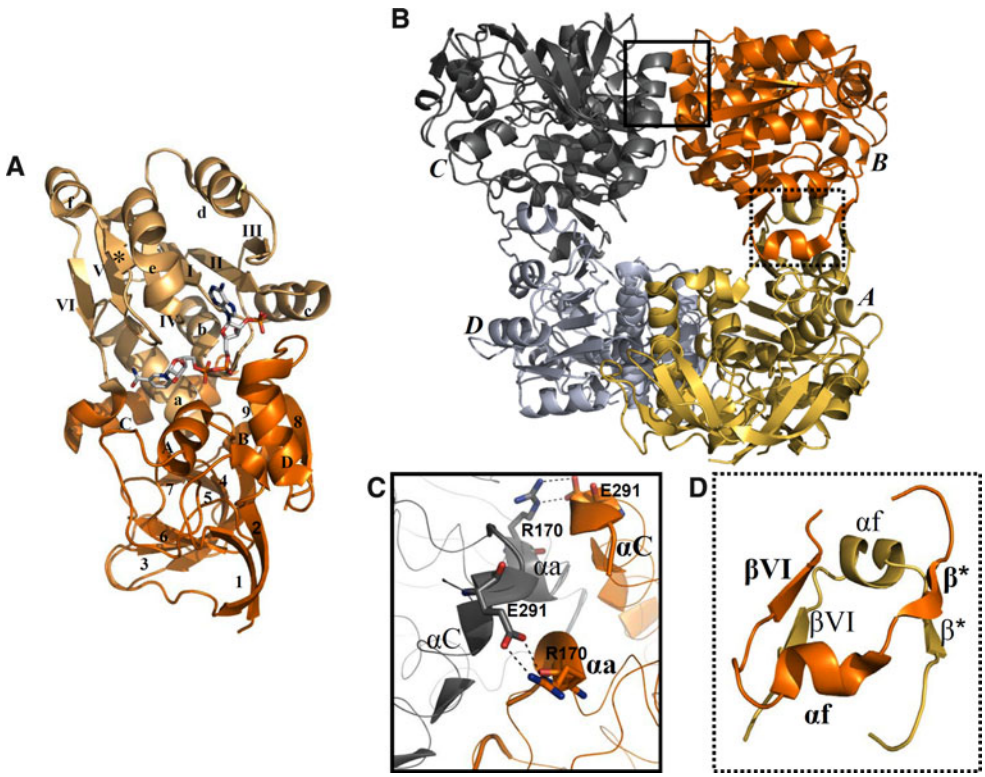

Fig. 3 Three-dimensional structure of human ζ-crystallin (PDB code 1YB5). **a** Tertiary structure of the monomer. The catalytic domain is coloured *dark orange* and the cofactor-binding domain is coloured *light orange*. The *β*-strands and α-helices of the cofactor-binding domain are indicated by *roman numerals* and *small letters*, respectively. Strand *β** is not part of the classical Rossmann fold topology. Nomenclature of the catalytic domain is in *Arabic numerals* and *capital letters*. **b** Quaternary structure. ζ-Crystallin consists of a tetramer that is a dimer of two identical dimers. The tetramer is generated by a crystallographic twofold symmetry, and the generated subunits are coloured *dark grey* and *light grey*, while the subunits from the asymmetric unit are coloured *dark orange* and *light orange*. The interface between the subunits in the dimer is highlighted with a *dotted square* and the interface between dimers in the tetramer is highlighted with a *full line square*. The residues implicated in the respective interfaces are displayed in the insets **c** and **d**

interaction in the dimer interface is a salt bridge and hydrogen bonds between Arg170 and Glu291 from each subunit (Fig. 3c).

Cofactor and putative substrate-binding sites

$NADP^+$ was located in the cleft between the catalytic and coenzyme binding domains of each subunit (Fig. 4a). As has been described for other QORs, the typical sequence motif GxGxx(G/A) in MDR enzymes is modified to GxxGxxG (Gly156-xx-Gly159-xx-Gly162). The adenine ring binds between the side chains of Leu225 and His200. This residue makes a hydrogen bond with the 2′-phosphate group of the adenine ribose, which is surrounded by the main chain of Ser158, Gly181 and Ala32, and the side chain of Arg201. This residue is at a salt bridge distance (3.86 Å) from the 2′-phosphate group. Similarly, in other QOR structures [9, 11, 12, 25], Gly, Tyr and a Lys or Arg, are residues that interact with the 2′-phosphate group and contribute to the preference for NADP. The pyrophosphate group establishes hydrogen bonds with the main chain of Gly160 and Val161, while nicotinamide ribose contacts with the hydroxyl group of Tyr53.

The pocket located between the $NADP^+$ molecule and the catalytic domain, where the C4 atom from the nicotinamide ring becomes accessible to the solvent (Fig. 4b), is a suitable site for substrate binding. In fact the pocket accommodates an acetate ion which may have come from the crystallization buffer. The pocket is formed by residues Asn48, Val50 and Tyr53 (αA), Tyr59 (loop αA-*β*4), Ile131 and Thr135 (αa), Ser248 and Arg249 (loop *β*IV-*β**), Thr270, Leu271 and Phe272 (αC) from subunit A, and Arg257*, Met260* and Ala261* (αf) from subunit B.

Docking simulations

To gain an understanding of how various substrates may bind to human ζ-crystallin, 2-hexenal, HHE and 3-nonen-2-one, displayed in Fig. 5, and 2-nonenal and HNE (data not shown), were docked into the active site. All substrates could be accommodated with their aliphatic chain making van der Waals interactions with Val50 in the inner part of

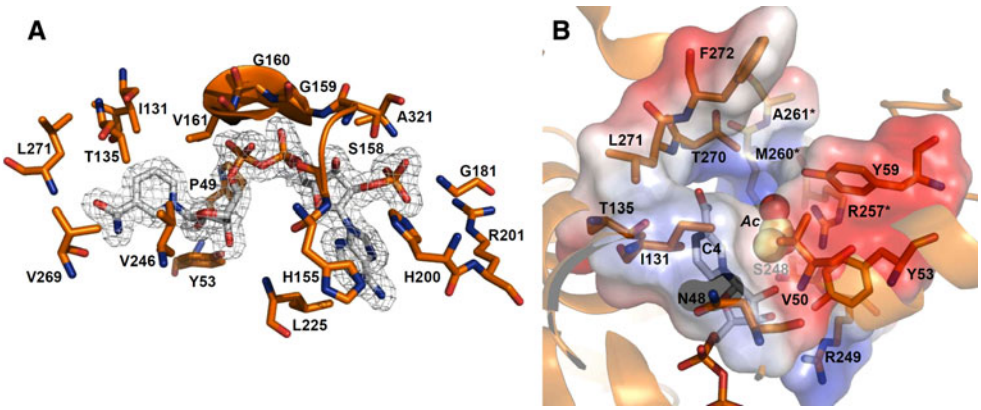

Fig. 4 Representation of the $NADP^+$-binding site and substrate-binding pocket in human ζ-crystallin. **a** $NADP^+$ molecule and the interacting protein residues. The electron density of $NADP^+$ is displayed at a contour level of 1.5 σ. The GxxGxxG structure is shown as a ribbon. **b** Image of main amino acid residues lining the putative substrate-binding cavity, which is shown as a surface. The $NADP^+$ molecule is displayed with its C4 atom in *black*. An acetate molecule (*Ac*) is accommodated near to $NADP^+$ supporting the suitability of this pocket to bind potential substrates

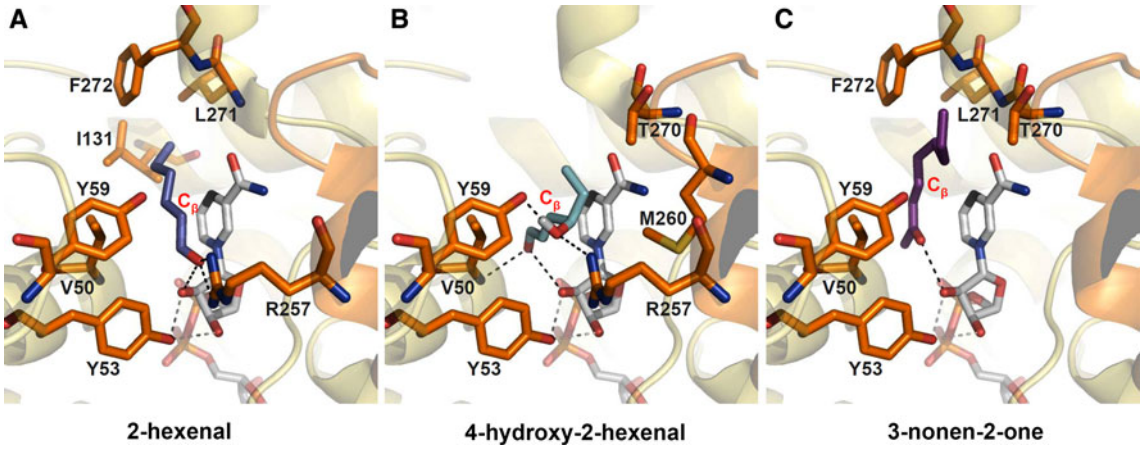

Fig. 5 Substrate docking simulations in the active site of human ζ-crystallin. Representations of the docking results for 2-hexenal (**a**), 4-hydroxy-2-hexenal (**b**) and 3-nonen-2-one (**c**). The main interacting residues are shown. The putative hydrogen bonds are represented as *black discontinuous lines*, while the crystallographic hydrogen bonds between Tyr53 and hydroxyl groups from the nicotinamide ribose are displayed as *grey discontinuous lines*. The atomic distances between the hydroxyl group of Tyr53 and the 2′- and 3′-hydroxyl groups of nicotinamide ribose are 2.71 and 2.95 Å, respectively. The distance between the C4 atom of $NADP^+$ (shown in *black*) and the C_β atom of the substrate is shorter than 4 Å

the substrate pocket. Tyr59, Thr270, Leu271 and Phe272 in the outer part of the pocket and Ile131 and Met260 in the inner part of the pocket are the residues that make van der Waals contacts with some substrates. On the other hand, substrates could establish hydrogen bonds through their carbonyl group (and the hydroxyl group in the case of HHE). Interestingly, all substrates seemed to interact through their carbonyl group with the 2′-hydroxyl of the nicotinamide ribose. Differences on other putative hydrogen bonds may explain the differences in the specific conformation of each substrate in the docking complex. Thus, the 2-hexenal carbonyl group appeared to be at hydrogen bond distance (2.05 Å) from the Arg257-NH1 group (Fig. 5a), while 3-nonen-2-one could not perform this interaction since its methyl group (C-1) might generate steric hindrance with Arg257 (Fig. 5c). In the case of HHE, the carbonyl group seemed to establish a hydrogen bond with the amide group of Val50 (2.25 Å) (Fig. 5b). Finally, the hydroxyl group of HHE would be at hydrogen bond distance from the Tyr59-OH (1.77 Å) and Arg257-NH1 (2.09 Å) groups (Fig. 5b). 2-Nonenal and HNE would establish the same interactions as 2-hexenal and HHE, respectively (data not shown).

Site-directed mutagenesis of substrate-pocket Tyr residues

It has been suggested for several Zn^{2+}-lacking MDRs that an active-site Tyr residue would act as an acid/base catalyst [26–29]. Therefore with the aim of studying their

potential role in AOR activity, Tyr residues in the active site, Tyr53 and Tyr59, were mutated, and kinetic constants were determined (Table 3). The Tyr53Phe mutant displayed a large increase in K_m values for all substrates and the cofactor, but mainly towards 3-buten-2-one and propenal with a 30-fold increase. In the case of 3-penten-2-one, 3-nonen-2-one, 2-hexenal and HHE, Tyr53Phe also showed a decrease in k_{cat}. On the other hand, the Tyr59Phe mutant exhibited almost the same kinetic parameter values as the wild-type enzyme for 2-alkenals, while the K_m increased for HHE. These results are consistent with the docking simulations (Fig. 5b) which indicated that Tyr59 would interact with the 4-hydroxyl group of HHE, an interaction that cannot be established with 2-alkenals.

Discussion

In the present study we described and characterized a novel enzymatic activity of human ζ-crystallin: the double bond α,β-hydrogenation of 2-alkenals and 3-alkenones. Thus, ζ-crystallin shows two distinct activities: QOR, which is used to name the protein family, and the novel activity, which is similar to that shown by the distantly related AOR protein family [30, 31]. Here we provide the first evidence of this activity in the QOR family. Only one mammalian enzyme from the AOR family, rat leukotriene B4 12-hydroxydehydrogenase (LTB4D), has been fully characterized in terms of kinetic constants and substrate specificity [32]. Comparison of the two enzymes shows similar substrate specificity, although with some differences. ζ-Crystallin is not active or is poorly active with cyclic and aromatic substrates, such as 2-cyclohexene-1-one, cinnamaldehyde or 15-ketoprostaglandin E_2, while LTB4D efficiently reduces prostaglandins and cinnamaldehyde. In general LTB4D prefers long-chain substrates (C12–C16) while ζ-crystallin seems to be more specific for medium-chain compounds (C4–C9), such as HHE or 3-buten-2-one. In all cases, rat LTB4D is more efficient than ζ-crystallin, with k_{cat}/K_m values from 6- to 50-fold higher for the best ζ-crystallin substrates, mostly due to higher k_{cat} values. The lack of kinetic data from the human LTB4D precludes establishing the relative physiological role of each enzyme in the human species.

The structural analysis showed that human ζ-crystallin is a homotetramer, which can be considered as a dimer of identical dimers, where subunits exhibit the classical MDR fold. A tetrameric structure for MDR proteins has already been described in Zn^{2+}-containing members of this superfamily, such as sorbitol dehydrogenase [33] and different alcohol dehydrogenases from bacteria and yeast [34, 35]. ζ-Crystallin represents the first described

Table 3 Kinetic analysis of human ζ-crystallin mutants

Substrate	Wild-type			Tyr53Phe			Tyr59Phe		
	K_m (μM)	k_{cat} (min^{-1})	k_{cat}/K_m (min^{-1} mM^{-1})	K_m (μM)	k_{cat} (min^{-1})	k_{cat}/K_m (min^{-1} mM^{-1})	K_m (μM)	k_{cat} (min^{-1})	k_{cat}/K_m (min^{-1} mM^{-1})
9,10-Phenanthrenequinone	1.5 ± 0.2[a]	130 ± 4[a]	87,000 ± 12,000[a]	10 ± 1	280 ± 16	28,000 ± 3,225	0.25 ± 0.01[b]	90 ± 9[b]	371,500 ± 137,000[b]
Propenal	1,450 ± 200	100 ± 4	70 ± 10	39,740 ± 3,560	140 ± 5.5	3.5 ± 0.3	860 ± 80	75 ± 2	90 ± 9
3-Buten-2-one	35 ± 3.5	10 ± 0.2	290 ± 30	970 ± 140	8 ± 0.2	8 ± 1	60 ± 3	17 ± 0.2	280 ± 14
3-Penten-2-one	535 ± 34	12 ± 0.2	22 ± 1.5	2,660 ± 480	4 ± 0.2	1.5 ± 0.3	n.d.	n.d.	n.d.
3-Nonen-2-one	940 ± 260	13 ± 1	14 ± 4	3,110 ± 390	3 ± 0.1	1 ± 0.1	n.d.	n.d.	n.d.
2-Hexenal	5,455 ± 620	17 ± 0.5	3.1 ± 0.4	73,270 ± 21,230	8 ± 1.5	0.1 ± 0.04	6,120 ± 600	22 ± 1	4 ± 0.4
4-Hydroxy-2-hexenal	130 ± 26	80 ± 5	613 ± 130	3,670 ± 2226	5 ± 2	1.4 ± 1	1,260 ± 320	130 ± 18	100 ± 30
NADPH	5 ± 0.7[a]			60 ± 4			15 ± 3		

n.d. not determined.

NADPH kinetics were determined with 6 mM 3-buten-2-one for the Tyr53Phe mutant, and with 20 μM 9,10-phenanthrenequinone for the Tyr59Phe mutant.

All aliphatic unsaturated compounds used as substrates exhibited the *trans* configuration.

Activities were determined in 0.1 M sodium phosphate, pH 7.0, with 0.15 mM NADPH (0.3 mM NADPH for the Tyr53Phe mutant) at 25°C.

[a] Fernández et al. [8].

[b] Porté et al. [12].

tetrameric structure for a Zn^{2+}-lacking MDR. As in other tetrameric MDR, the interface between dimers is mainly stabilized by two salt bridges between each monomer pair. The residues implicated belong to the catalytic domain (Arg170) and coenzyme-binding domain (Glu291), which make the only bond in this interface. This may explain the relative weakness of this interaction, which is broken by high ionic strength.

The analysis of human ζ-crystallin structure provides information for the identification of essential residues for the enzymatic activity. In other Zn^{2+}-lacking MDRs, e.g. *Candida tropicalis*, yeast and human enoyl reductase [28, 29], *Arabidopsis* NADP-dependent oxidoreductase P1 [27], human prostaglandin reductase 2 (PGR-2) [36] and guinea pig LTB4D [26], structural and mutagenesis data support the participation of a Tyr residue in their catalytic mechanism. In the substrate-binding site of ζ-crystallin, Tyr59 and Tyr53 are in an appropriate location for catalysis. A previous mutagenesis study on the role of Tyr59 in quinone reduction supports participation in substrate binding [12]. Here we have extended the study to the function of the two Tyr in the AOR activity. The Tyr53Phe mutant displayed an increase in K_m and a decrease in k_{cat} for most substrates, resulting in a 14- to 440-fold drop in catalytic efficiency, and supporting a contribution of Tyr53 in the substrate binding/catalytic mechanism of double-bond hydrogenation of alkenals and alkenones. Similar results and conclusions have been reported for the Tyr mutagenesis studies of AOR members (Tyr245 in LTB4D [37] and Tyr259 in PGR-2 [38]) involved in the reduction of the same substrate types. Tyr245 and Tyr259 are located in homologous positions in the primary sequence, while Tyr53 is not. Interestingly, these active-site tyrosine residues in ζ-crystallin and AORs do not directly bind to the carbonyl group of the substrate (present results; [26, 36]), and therefore they cannot be involved in acid/base catalysis. However, in all cases they interact through a hydrogen bond with the 2′-hydroxyl of nicotinamide ribose of $NADP^+$. Moreover, docking simulations indicate that the carbonyl group of the substrates also interacts with the 2′-hydroxyl of nicotinamide ribose in both enzyme types (present results; [26, 27, 36]). For AORs it has been proposed that the Tyr may act together with 2′-hydroxyl of nicotinamide ribose in the stabilization of the enolate form of the transition-state intermediate [26, 27]. In spite of the large overall structural differences with AORs (20–25% sequence identity), a similar catalytic mechanism may be proposed for ζ-crystallin (Fig. 6) because of the common

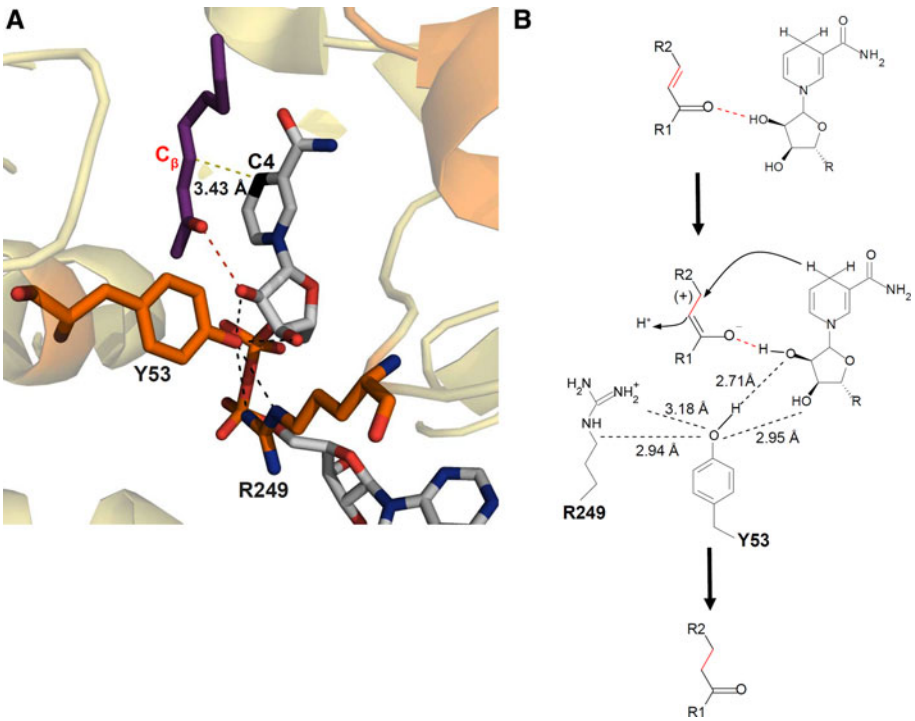

Fig. 6 Representation of the environment of Tyr53 and of a putative catalytic mechanism for the reduction of the α,β-unsaturated bond of alkenal/one. **a** Tyr53 makes hydrogen bonds with 2′- and 3′-hydroxyl groups of nicotinamide ribose, and NH1 and Nε groups of Arg249, in the crystal structure (*black dotted lines*). The predicted hydrogen bond between docked 3-nonen-2-one and the 2′-hydroxyl of nicotinamide ribose is displayed as a *red dotted line*. The distance between C4 of nicotinamide and C_β of the substrate is indicated as a *green dotted line*. **b** The catalytic mechanism requires the formation of an enolate anion which may be stabilized by the hydrogen bond with the 2′-hydroxyl of nicotinamide ribose, as proposed for the AOR enzymes [26, 36]. Tyr53 may potentiate the catalytic role of the 2′-hydroxyl group

active-site structural features and substrate specificity. The environment of Tyr53 (Fig. 6a) may facilitate its potential participation in the catalytic mechanism (Fig. 6b). The interaction of Tyr53 with Arg249 would lower the *p*Ka value of the Tyr53 hydroxyl group, therefore enabling the 2′-hydroxyl of nicotinamide ribose to stabilize the transition-state intermediate (enolate anion). Thus, participation of Tyr53 in catalysis seems only indirect, which would explain the moderate effect of the Tyr53Phe mutation on the k_{cat} values. The mutation increases K_m values, especially for the short-chain substrates, which would be also an indirect consequence of the hydrophobic change on the active-site environment.

Tyr59Phe mutant does not change the kinetic parameters for the majority of the substrates but, remarkably, the mutation produces a tenfold increase in the K_m value for HHE, suggesting a specific interaction of Tyr59 with this physiological substrate. The docking simulation suggests a hydrogen bond between the hydroxyl groups of Tyr59 and HHE. This interaction appears essential for the higher specificity with this substrate, which exhibits a 42-fold lower K_m value as compared to that of 2-hexenal, and therefore the enzyme is especially relevant for elimination of this product of lipid peroxidation.

Neither Tyr53 nor Tyr59 seems to be essential for QOR activity, suggesting a different mechanism for quinone reduction. There are several examples of enzymes that catalyse quinone reduction, where the substitution of the putative catalytic residue does not affect quinone reducing activity [12, 39–42]. In the case of human PIG3, the Tyr59 homologue, Tyr51, is not essential for catalysis either [12]. Similarly, the catalytic mechanism for the QOR activity of ζ-crystallin may be only based on orientation and proximity effects as already suggested [12].

Several physiological roles have been proposed for ζ-crystallin. A structural role in the lens of some vertebrate species has been well documented [3, 43, 44]. Moreover, it has been recently reported that ζ-crystallin plays an important function in the regulation of protein levels of bcl-2 and BSC-1 through modulating their mRNA stability [17, 18]. These studies reinforce the previously proposed role of ζ-crystallin as an RNA-binding protein [8, 15, 16]. Evidence also indicates a well-conserved catalytic role of ζ-crystallin. Thus, when sequences of three evolutionarily related structures, ζ-crystallin, yeast Zta1p and *E. coli* QOR, are compared, the substrate-binding pocket is significantly conserved, with much higher sequence identity (40%) than that of other parts of the molecule, including the cofactor-binding site (28%) [45]. Interestingly, all members of the ζ-crystallin subfamily exhibit a Tyr residue at each of the two positions homologous to Tyr53 and Tyr59, and their three-dimensional localization in the *E. coli* QOR structure [9] is identical to that in ζ-crystallin. The conserved structure is consistent with the demonstrated catalytic activity towards quinones for the three enzymes. In addition, the conservation of the active-site tyrosines, much more involved in alkenal/one reduction than in the activity with quinones, predicts that the former activity is also general in the ζ-crystallin subfamily. Finally, Tyr53 in ζ-crystallin is similarly positioned and functionally equivalent to Tyr245 and Tyr259 in AOR members, supporting convergent molecular evolution.

A variety of aldo–keto reductases and short-chain dehydrogenases/reductases, with well-established physiological substrates, e.g. steroids and prostaglandins [46, 47], exhibit the highest activity with quinones [47, 48], although this function is not considered to have a major physiological role. In fact, other enzymes exist, such as NAD(P)H:quinone oxidoreductase (NQO1), which are much more specific and active towards quinones [49]. Similarly, the AOR activity of ζ-crystallin may be of more physiological significance than the quinone reduction. The best alkenal substrates for ζ-crystallin are HNE and, especially, HHE, which are the major alkenal products of the lipid peroxidation pathway for *n*-6 and *n*-3 polyunsaturated fatty acids, respectively [50]. While HNE is a well-known toxic compound, HHE has been recently shown to be even more potent than HNE in eliciting cellular responses and, in some human tissues, HHE adducts have been found at higher levels than the corresponding HNE conjugates [51], stressing the pathological relevance of HHE. ζ-Crystallin seems well suited to contribute to the inactivation of this toxic compound.

In conclusion, ζ-crystallin appears to be a multifunctional protein with a structural role in the eye, RNA-binding properties and quinone reductase activity. The 2-alkenal/3-alkenone reductase activity here described adds further insights and complexity into this Zn^{2+}-lacking subfamily of MDRs.

Acknowledgments We acknowledge Dr. M.J. Ibarz (Servei d'Anàlisi Química, Universitat Autònoma de Barcelona, Spain) for the GC/MS analysis. We thank Dr. Ignacio Fita for his kind advice and for allowing some of the computer modelling studies to be performed in his laboratory. This work was supported by grants from the Spanish Dirección General de Investigación (BFU2008-02945) and Generalitat de Catalunya (2009 SGR795). The Structural Genomics Consortium is a registered charity (number 1097737) receiving funds from the Canadian Institutes for Health Research, the Canadian Foundation for Innovation, Genome Canada through the Ontario Genomics Institute, GlaxoSmithKline, Karolinska Institutet, the Knut and Alice Wallenberg Foundation, the Ontario Innovation Trust, the Ontario Ministry for Research and Innovation, Merck & Co., the Novartis Research Foundation, the Swedish Agency for Innovation Systems, the Swedish Foundation for Strategic Research and the Wellcome Trust. The project was supported by the Oxford NIHR Musculoskeletal Biomedical Research Unit.

References

1. Persson B, Hedlund J, Jörnvall H (2008) Medium- and short-chain dehydrogenase/reductase gene and protein families: the MDR superfamily. Cell Mol Life Sci 65:3879–3894
2. Huang QL, Russell P, Stone SH, Zigler JS Jr (1987) Zeta-crystallin, a novel lens protein from the guinea pig. Curr Eye Res 6:725–732
3. Rodriguez IR, González P, Zigler JS Jr, Borras T (1992) A guinea-pig hereditary cataract contains a splice-site deletion in a crystallin gene. Biochim Biophys Acta 1180:44–52
4. Rao PV, Krishna CM, Zigler JS Jr (1992) Identification and characterization of the enzymatic activity of zeta-crystallin from guinea pig lens. A novel NADPH:quinone oxidoreductase. J Biol Chem 267:96–102
5. Jörnvall H, Persson B, Du Bois GC, Lavers GC, Chen JH, González P, Rao PV, Zigler JS Jr (1993) Zeta-crystallin versus other members of the alcohol dehydrogenase super-family. Variability as a functional characteristic. FEBS Lett 322:240–244
6. Nordling E, Jörnvall H, Persson B (2002) Medium-chain dehydrogenases/reductases (MDR). Family characterizations including genome comparisons and active site modeling. Eur J Biochem 269:4267–4276
7. Riveros-Rosas H, Julián-Sánchez A, Villalobos-Molina R, Pardo JP, Pina E (2003) Diversity, taxonomy and evolution of medium-chain dehydrogenase/reductase superfamily. Eur J Biochem 270:3309–3334
8. Fernández MR, Porté S, Crosas E, Barberà N, Farrés J, Biosca JA, Parés X (2007) Human and yeast zeta-crystallins bind AU-rich elements in RNA. Cell Mol Life Sci 64:1419–1427
9. Thorn JM, Barton JD, Dixon NE, Ollis DL, Edwards KJ (1995) Crystal structure of Escherichia coli QOR quinone oxidoreductase complexed with NADPH. J Mol Biol 249:785–799
10. Maruyama A, Kumagai Y, Morikawa K, Taguchi K, Hayashi H, Ohta T (2003) Oxidative-stress-inducible qorA encodes an NADPH-dependent quinone oxidoreductase catalysing a one-electron reduction in Staphylococcus aureus. Microbiology 149:389–398
11. Shimomura Y, Kakuta Y, Fukuyama K (2003) Crystal structures of the quinone oxidoreductase from Thermus thermophilus HB8 and its complex with NADPH: implication for NADPH and substrate recognition. J Bacteriol 185:4211–4218
12. Porté S, Valencia E, Yakovtseva EA, Borràs E, Shafqat N, Debreczeny JE, Pike AC, Oppermann U, Farrés J, Fita I, Parés X (2009) Three-dimensional structure and enzymatic function of proapoptotic human p53-inducible quinone oxidoreductase PIG3. J Biol Chem 284:17194–17205
13. Gagna CE, Chen JH, Kuo HR, Lambert WC (1998) Binding properties of bovine ocular lens zeta-crystallin to right-handed B-DNA, left-handed Z-DNA, and single-stranded DNA. Cell Biol Int 22:217–225
14. Kranthi BV, Balasubramanian N, Rangarajan PN (2006) Isolation of a single-stranded DNA-binding protein from the methylotrophic yeast, Pichia pastoris and its identification as zeta crystallin. Nucleic Acids Res 34:4060–4068
15. Tang A, Curthoys NP (2001) Identification of zeta-crystallin/NADPH:quinone reductase as a renal glutaminase mRNA pH response element-binding protein. J Biol Chem 276:21375–21380
16. Schroeder JM, Liu W, Curthoys NP (2003) pH-responsive stabilization of glutamate dehydrogenase mRNA in LLC-PK1-F+ cells. Am J Physiol Renal Physiol 285:F258–F265
17. Lapucci A, Lulli M, Amedei A, Papucci L, Witort E, Di Gesualdo F, Bertolini F, Brewer G, Nicolin A, Bevilacqua A, Schiavone N, Morello D, Donnini M, Capaccioli S (2010) zeta-Crystallin is a bcl-2 mRNA binding protein involved in bcl-2 overexpression in T-cell acute lymphocytic leukemia. FASEB J 24:1852–1865
18. Szutkowska M, Vernimmen C, Debaix H, Devuyst O, Friedlander G, Karim Z (2009) Zeta-crystallin mediates the acid pH-induced increase of BSC1 cotransporter mRNA stability. Kidney Int 76:730–738
19. Emsley P, Cowtan K (2004) Coot: model-building tools for molecular graphics. Acta Crystallogr D Biol Crystallogr 60:2126–2132
20. Krissinel E, Henrick K (2007) Inference of macromolecular assemblies from crystalline state. J Mol Biol 372:774–797
21. Dundas J, Ouyang Z, Tseng J, Binkowski A, Turpaz Y, Liang J (2006) CASTp: computed atlas of surface topography of proteins with structural and topographical mapping of functionally annotated residues. Nucleic Acids Res 34:W116–W118
22. Goodsell DS, Morris GM, Olson AJ (1996) Automated docking of flexible ligands: applications of AutoDock. J Mol Recognit 9:1–5
23. McConkey BJ, Sobolev V, Edelman M (2002) The performance of current methods in ligand-protein docking. Curr Sci 83:845–855
24. Duhaiman AS, Rabbani N, AlJafari AA, Alhomida AS (1995) Purification and characterization of zeta-crystallin from the camel lens. Biochem Biophys Res Commun 215:632–640
25. Pan X, Zhang H, Gao Y, Li M, Chang W (2009) Crystal structures of Pseudomonas syringae pv. tomato DC3000 quinone oxidoreductase and its complex with NADPH. Biochem Biophys Res Commun 390:597–602
26. Hori T, Yokomizo T, Ago H, Sugahara M, Ueno G, Yamamoto M, Kumasaka T, Shimizu T, Miyano M (2004) Structural basis of leukotriene B4 12-hydroxydehydrogenase/15-oxo-prostaglandin 13-reductase catalytic mechanism and a possible Src homology 3 domain binding loop. J Biol Chem 279:22615–22623
27. Youn B, Kim SJ, Moinuddin SG, Lee C, Bedgar DL, Harper AR, Davin LB, Lewis NG, Kang C (2006) Mechanistic and structural studies of apoform, binary, and ternary complexes of the Arabidopsis alkenal double bond reductase At5g16970. J Biol Chem 281:40076–40088
28. Airenne TT, Torkko JM, Van den Plas S, Sormunen RT, Kastaniotis AJ, Wierenga RK, Hiltunen JK (2003) Structure-function analysis of enoyl thioester reductase involved in mitochondrial maintenance. J Mol Biol 327:47–59
29. Chen ZJ, Pudas R, Sharma S, Smart OS, Juffer AH, Hiltunen JK, Wierenga RK, Haapalainen AM (2008) Structural enzymological studies of 2-enoyl thioester reductase of the human mitochondrial FAS II pathway: new insights into its substrate recognition properties. J Mol Biol 379:830–844
30. Mano J, Torii Y, Hayashi S, Takimoto K, Matsui K, Nakamura K, Inze D, Babiychuk E, Kushnir S, Asada K (2002) The NADPH:quinone oxidoreductase P1-zeta-crystallin in Arabidopsis catalyzes the alpha, beta-hydrogenation of 2-alkenals: detoxication of the lipid peroxide-derived reactive aldehydes. Plant Cell Physiol 43:1445–1455
31. Dick RA, Kensler TW (2004) The catalytic and kinetic mechanisms of NADPH-dependent alkenal/one oxidoreductase. J Biol Chem 279:17269–17277
32. Dick RA, Kwak MK, Sutter TR, Kensler TW (2001) Antioxidative function and substrate specificity of NAD(P)H-dependent alkenal/one oxidoreductase. A new role for leukotriene B4 12-hydroxydehydrogenase/15-oxoprostaglandin 13-reductase. J Biol Chem 276:40803–40810
33. Pauly TA, Ekstrom JL, Beebe DA, Chrunyk B, Cunningham D, Griffor M, Kamath A, Lee SE, Madura R, McGuire D, Subashi T, Wasilko D, Watts P, Mylari BL, Oates PJ, Adams PD, Rath VL (2003) X-ray crystallographic and kinetic studies of human sorbitol dehydrogenase. Structure 11:1071–1085

34. Shimon LJ, Goihberg E, Peretz M, Burstein Y, Frolow F (2006) Structure of alcohol dehydrogenase from Entamoeba histolytica. Acta Crystallogr D Biol Crystallogr 62:541–547
35. Levin I, Meiri G, Peretz M, Burstein Y, Frolow F (2004) The ternary complex of Pseudomonas aeruginosa alcohol dehydrogenase with NADH and ethylene glycol. Protein Sci 13:1547–1556
36. Wu YH, Ko TP, Guo RT, Hu SM, Chuang LM, Wang AH (2008) Structural basis for catalytic and inhibitory mechanisms of human prostaglandin reductase PTGR2. Structure 16:1714–1723
37. Bougioukou DJ, Stewart JD (2008) Opposite stereochemical courses for enzyme-mediated alkene reductions of an enantiomeric substrate pair. J Am Chem Soc 130:7655–7658
38. Chou WL, Chuang LM, Chou CC, Wang AH, Lawson JA, Fitzgerald GA, Chang ZF (2007) Identification of a novel prostaglandin reductase reveals the involvement of prostaglandin E2 catabolism in regulation of peroxisome proliferator-activated receptor gamma activation. J Biol Chem 282:18162–18172
39. Ma Q, Cui K, Xiao F, Lu AY, Yang CS (1992) Identification of a glycine-rich sequence as an NAD(P)H-binding site and tyrosine 128 as a dicumarol-binding site in rat liver NAD(P)H:quinone oxidoreductase by site-directed mutagenesis. J Biol Chem 267:22298–22304
40. Kim IK, Yim HS, Kim MK, Kim DW, Kim YM, Cha SS, Kang SO (2008) Crystal structure of a new type of NADPH-dependent quinone oxidoreductase (QOR2) from Escherichia coli. J Mol Biol 379:372–384
41. Fujii Y, Watanabe K, Hayashi H, Urade Y, Kuramitsu S, Kagamiyama H, Hayaishi O (1990) Purification and characterization of rho-crystallin from Japanese common bullfrog lens. J Biol Chem 265:9914–9923
42. Schlegel BP, Ratnam K, Penning TM (1998) Retention of NADPH-linked quinone reductase activity in an aldo-keto reductase following mutation of the catalytic tyrosine. Biochemistry 37:11003–11011
43. Garland D, Rao PV, Del Corso A, Mura U, Zigler JS Jr (1991) zeta-Crystallin is a major protein in the lens of Camelus dromedarius. Arch Biochem Biophys 285:134–136
44. Fujii Y, Kimoto H, Ishikawa K, Watanabe K, Yokota Y, Nakai N, Taketo A (2001) Taxon-specific zeta-crystallin in Japanese tree frog (Hyla japonica) lens. J Biol Chem 276:28134–28139
45. Porté S, Crosas E, Yakovtseva E, Biosca JA, Farrés J, Fernández MR, Parés X (2009) MDR quinone oxidoreductases: the human and yeast zeta-crystallins. Chem Biol Interact 178:288–294
46. Penning TM, Steckelbroeck S, Bauman DR, Miller MW, Jin Y, Peehl DM, Fung KM, Lin HK (2006) Aldo-keto reductase (AKR) 1C3: role in prostate disease and the development of specific inhibitors. Mol Cell Endocrinol 248:182–191
47. Chung HS, Harvey RG, Armstrong RN, Jarabak J (1987) Polycyclic aromatic hydrocarbon quinones and glutathione thioethers as substrates and inhibitors of the human placental NADP-linked 15-hydroxyprostaglandin dehydrogenase. J Biol Chem 262:12448–12451
48. Byrns MC, Steckelbroeck S, Penning TM (2008) An indomethacin analogue, N-(4-chlorobenzoyl)-melatonin, is a selective inhibitor of aldo-keto reductase 1C3 (type 2 3alpha-HSD, type 5 17beta-HSD, and prostaglandin F synthase), a potential target for the treatment of hormone dependent and hormone independent malignancies. Biochem Pharmacol 75:484–493
49. Giulivi C, Cadenas E (1994) One- and two-electron reduction of 2-methyl-1,4-naphthoquinone bioreductive alkylating agents: kinetic studies, free-radical production, thiol oxidation and DNA-strand-break formation. Biochem J 301:21–30
50. Catalá A (2009) Lipid peroxidation of membrane phospholipids generates hydroxy-alkenals and oxidized phospholipids active in physiological and/or pathological conditions. Chem Phys Lipids 157:1–11
51. Long EK, Picklo MJ Sr (2010) Trans-4-hydroxy-2-hexenal, a product of n-3 fatty acid peroxidation: make some room HNE. Free Radic Biol Med 49:1–8